Proceedings of the 17th World Congress
The International Federation of Automatic Control
Seoul, Korea, July 6-11, 2008

Structure Improvement of an XY Flexure Micromanipulator for Micro/Nano Scale Manipulation ⋆

Qingsong Xu * **Yangmin Li** **

* *Department of Electromechanical Engineering, Faculty of Science and Technology, University of Macau, Macao SAR, P. R. China, (e-mail: ya47401@umac.mo).*
** *Department of Electromechanical Engineering, Faculty of Science and Technology, University of Macau, Macao SAR, P. R. China, (e-mail: ymli@umac.mo).*

Abstract: An effort made towards the performance improvement for an XY micromanipulator featuring parallel architecture and flexure hinges has been presented in this paper. Through the implementation of four steps evolution of the original structure, a new manipulator with decoupled motion is finally obtained, which owns an enlarged workspace and eliminated stiffening and buckling phenomena. The merits of the new manipulator have been illustrated via the finite element analysis performed via ANSYS software package. It is believed that the generated flexure micromanipulator can be adopted in the applications involving manipulation of objects in micro- and nano-meter scales.

1. INTRODUCTION

The manipulation of objects in micro and nano sales is indispensable in many research and application fields such as micro-component assembly in semiconductor industry, DNA manipulation in biotechnology, and atom handling in nanotechnology, etc. As a consequence, the manipulators with ultrahigh precision and rapid response are in great demand nowadays (Sievers and Fatikow [2006]).

In order to meet the aforementioned requirements, the manipulators themselves may be designed to possess sizes in macro scale (tens or hundreds of millimeters) with fine performance. Generally, precision manipulators employ flexure joints instead of conventional mechanical joints. Flexure hinges can provide the manipulator with a small scale motion by utilizing the elasticity of adopted materials. Moreover, they have major merits in terms of vacuum compatibility, no backlash property, no nonlinear friction and free of lubrication, and simple mechanical structure.

In addition, the flexure manipulators are usually designed based upon parallel mechanisms but not serial ones (Pernette et al. [1997]). Not like a serial manipulator whose end-effector is connected to the base by a series of links and joints in serial, a parallel manipulator has such an advantage that the end-effector (or mobile platform) is attached to the fixed base by more than one limb together, where each limb usually is a serial kinematic chain. This unique merit endows a parallel mechanism with attractive advantages for high precision application, since the manipulator possesses less cumulative errors in the end-effector and higher stiffness than a traditional serial manipulator. Besides, since more than one joint/actuator can be assembled on the base, a parallel manipulator generally owns lighter mass of moving components (Merlet [2000]). Hence, a higher natural frequency can be attained by a compliant parallel manipulator (CPM) utilizing parallel structure and flexure hinges, which indicates a quicker dynamic response as well.

Up to now, many CPMs have been designed for micro and nano scale manipulation proposed by Ryu et al. [1997], Tanikawa and Arai [1999], Chen et al. [2002], Yi et al. [2003], Lu et al. [2004], Oh et al. [2005], Tang and Chen [2006], Xu and Li [2007], etc., to illustrate just a few. In particular, several XY micromanipulators which can provide two translations along the x- and y-axes have been proposed due to the potential application of XY stages concerning surface scanning, cell injection, and so on (See Li and Xu [2006], Yao et al. [2007], Choi et al. [2007]).

In previous works of the authors, a novel XY CPM is designed and presented (see Li and Xu [2006]), which possesses a relatively simple structure than other ones. As an initial design, it has been recently noticed that the original CPM exhibits several disadvantages in terms of stiffening, buckling, and parasitic motion, etc., which may prevent its application in micro/nano manipulation fields. Motivated by these problems, the original XY CPM structure is improved to enhance its performances as conducted in details in the following discussions.

2. ARCHITECTURE DESCRIPTION OF AN XY CPM

The original 2-DOF CPM is shown in Fig. 1. It employs flexure hinges at all joints, and consists of a mobile platform, a fixed base and two limbs with identical kinematic structure. Each limb connects the mobile platform to the fixed base by a parallelogram structure including four

⋆ This work was supported by the Research Committee of University of Macau under Grant RG065/06-07S/08T/LYM/FST and Macao Science and Technology Development Fund under Grant 069/2005/A.

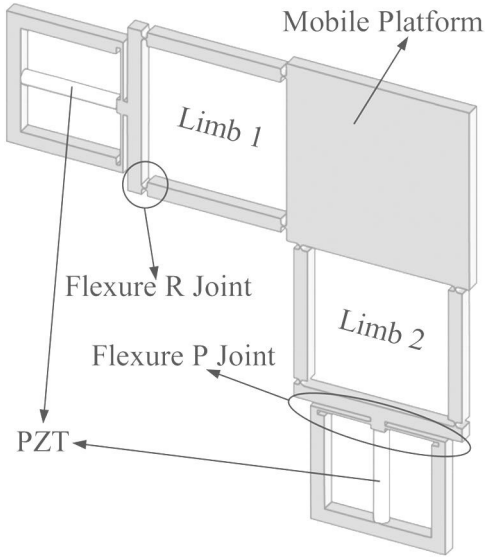

Fig. 1. The original 2-DOF CPM.

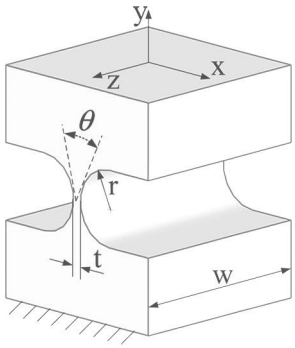

Fig. 2. Parameters of the flexure R hinge.

flexure revolute (R) hinges (Fig. 2) and a flexure prismatic (P) hinge (Fig. 3) in sequence. The first P joint within each limb is fixed at the base and actuated by a piezoelectric actuator (PZT). With mounting a suitable end-effector on the mobile platform or placing the platform under a specified microscope as an XY-table, the CPM can be used in 2-D micro/nano scale positioning application. And this type of CPM has been proposed by Li and Xu [2006], where the initial selections of actuators and materials to develop the CPM were also presented.

However, it has been found that this preliminary version of CPM exhibits several disadvantages, which may prevent its application in micro/nano manipulation fields. To deal with such a problem, the original structure of the stage is modified in the following section.

3. DESIGN IMPROVEMENT OF THE STAGE

The original XY CPM is modified in terms of four steps as enumerated below.

3.1 Step 1: Modify the actuation joint

In the first step, we modify the type of the original actuation P joint to reduce stiffening phenomenon.

Assume that the deflection of the original actuated flexure P joint only comes from the two leaves. With reference

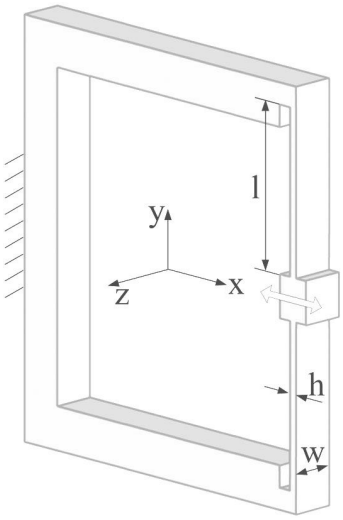

Fig. 3. Parameters of the actuated flexure P joint.

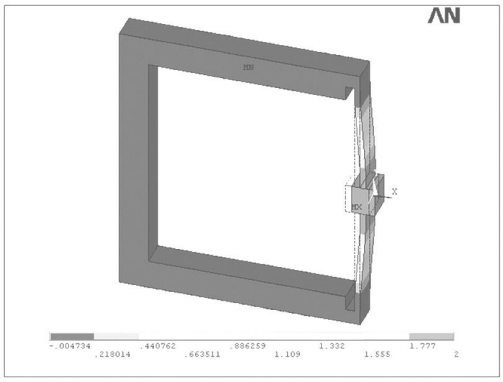

Fig. 4. Deflection of the actuated flexure P ioint.

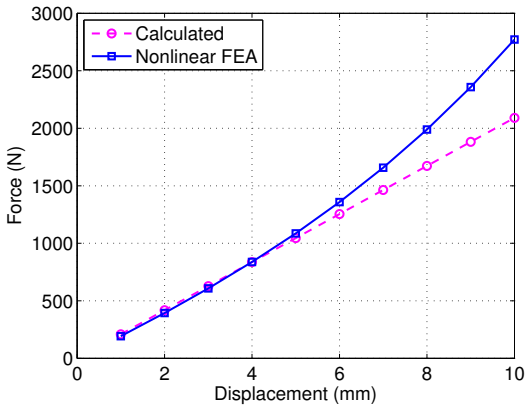

Fig. 5. Force-displacement relationship of actuated P joint.

to Fig. 3, its structural stiffness in actuation direction (x-axis) can be easily calculated as:

$$K_1 = \frac{2Ewh^3}{l^3} \ . \tag{1}$$

Once driven by a PZT, the two leaves of the flexure P joint suffer from axial direction loads in the y direction in addition to the forces along x direction (Fig. 3). The exerted axial loads are the sources of stress stiffening phenomenon in the flexure P joint. To demonstrate the stiffening effect, the finite element analysis (FEA) of

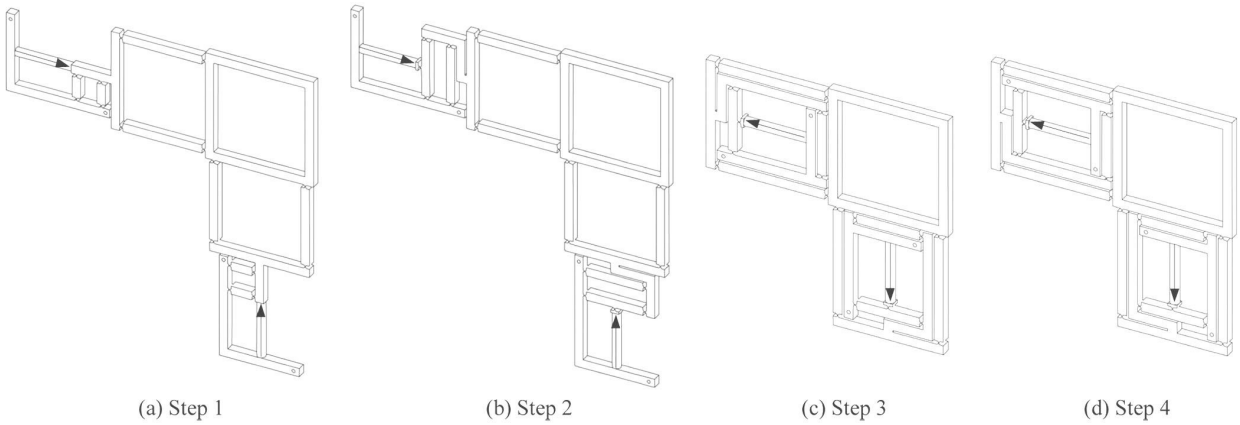

Fig. 6. Structure evolution processes for the XY stage.

the P joint is performed in ANSYS environment with architectural parameters of $w = 10\,\text{mm}$, $l = 38\,\text{mm}$, and $h = 2\,\text{mm}$. The Al 7075 alloy is selected as the material.

By applying forces at the input end of the flexure joint and monitoring the induced displacement, the force-displacement curves are plotted in Fig. 5, where the non-linear analysis is carried out with the consideration of the stress stiffening. The curves of the FEA results reveal that the stiffening phenomenon increases the actuation stiffness of the flexure P joint, which may reduce the output stroke of PZT and the workspace of CPM correspondingly.

Hence, in order to diminish the effect of stress stiffening, the actuation P joint is modified as shown in Fig. 6(a), where the axial loads can be avoided.

3.2 Step 2: Add a lever mechanism

The main drawback of PZT is its limited stroke, which leads to a small workspace of the CPM. Thus, for the sake of enlarging the CPM workspace as required, the PZT stroke is amplified by utilizing a lever amplification mechanism as illustrated in Fig. 6(b).

Assume that the PZT possesses a stroke of Q and resolution of Δ. With a selection of the amplification ratio A for the lever mechanism, the PZT stroke can be enlarged to AQ, while its resolution is reduced to Δ/A accordingly. Therefore, a tradeoff between stroke and resolution values is usually considered in the design of the lever mechanism in accordance with the application requirements.

In addition, some other types of lever mechanisms can also be adopted for the amplification of the PZT travel as well.

3.3 Step 3: Reverse the actuation direction

Next, we reverse the actuation direction to reduce the risk of buckling in all flexure R joints.

Buckling may occur in the flexure hinges once their axial loads are compressive. Observing one limb of the CPM in Fig. 1 reveals that when one PZT pushes the leaf-based P joint, the four flexure hinges in the same limb, all bear the axial compressive load. So, buckling phenomenon may arise, which may lead to instability of the CPM and restrict the CPM workspace as well.

In order to diminish buckling in the CPM, the concept of reverse actuation is adopted here. By inverting the actuation direction, the flexure R hinges constructing the parallelogram in one CPM limb are all suffering from axial tensile loads instead. And the notch hinges in the actuation P joint do not bear only axial compressive loads either. Consequently, the buckling can be excluded from the modified CPM.

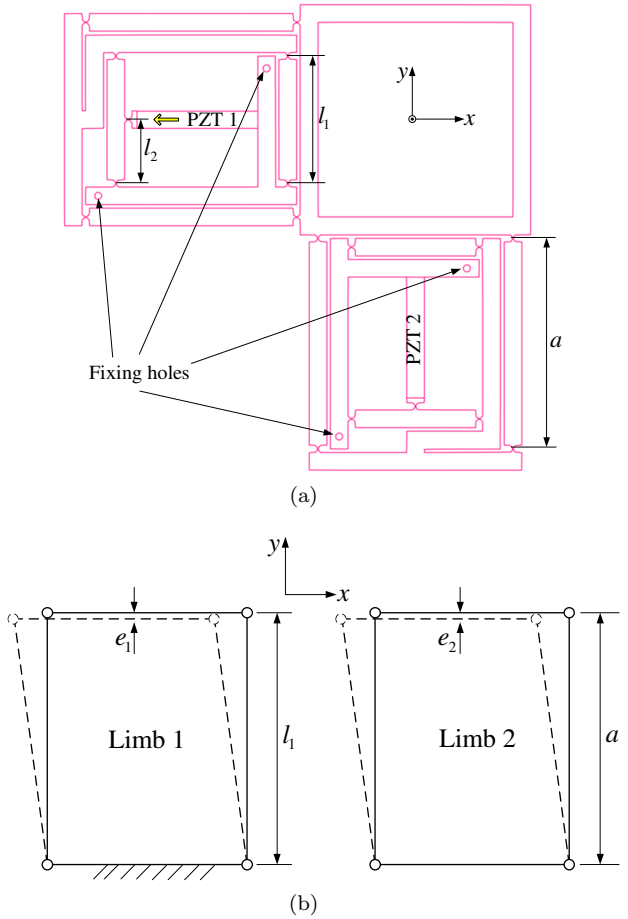

Fig. 7. Representation of parasitic translations.

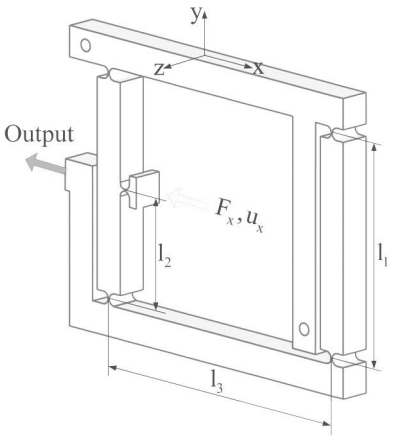

Fig. 8. Parameters of the modified flexure P joint.

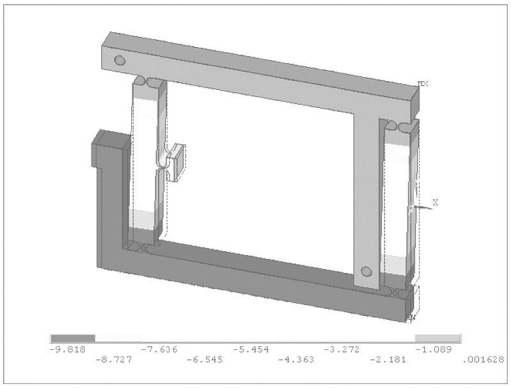

Fig. 9. Deflection of the modified P joint.

Moreover, in order to make fully use of the limited space to build a compact CPM, the amplification P joint is inscribed into the parallelogram as shown in Fig. 6(c).

3.4 Step 4: Change the assembly model

In this step, we change the assembly model of the two limbs so as to diminish the parasitic motion or crosstalk of the CPM between the two working directions.

With limb 1 of the CPM in Fig. 6(c) driven by a PZT, the connecting rods subjected to deflections are shown in Fig. 7(a). Meanwhile, the induced parasitic motions of the two limbs are elaborated in Fig. 7(b). It is observed that the parasitic translations e_1 and e_2 introduced by limb 1 and limb 2 are both along the same $(-y)$ direction.

Hence, in order to reduce the parasitic motion of the CPM, e_1 and e_2 should be designed to be along the reverse direction if possible. Thus, the assembly model of the two limbs is revised as shown in Fig. 6(d), where the two limbs are assembled in reverse with comparison to the CPM structure in Fig. 6(c).

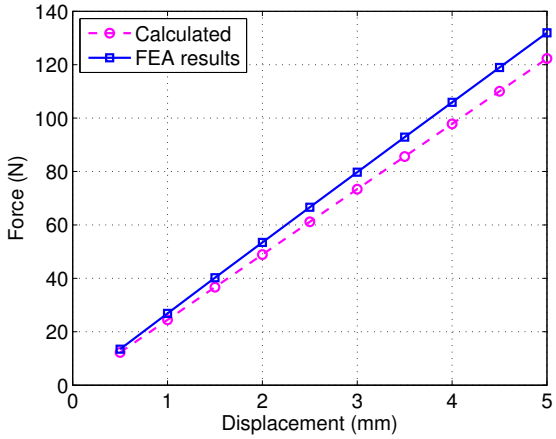

Fig. 10. Force-displacement relationship of modified P joint.

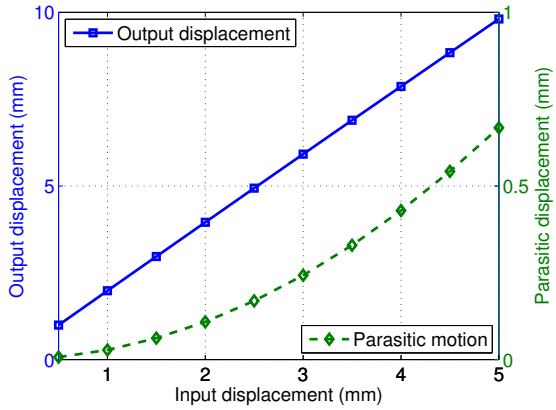

Fig. 11. Input and output motion relationship of modified P joint.

4. PERFORMANCE VALIDATION OF THE IMPROVED XY CPM

4.1 Performance of the amplification P joint

As far as the modified flexure P joint (see Fig. 8) is concerned, assume the deflection only comes from the notch hinges. Then, its actuation stiffness in the x-axis direction can be calculated as follows.

Let the force and displacement created by the PZT be F_x and u_x, respectively, which are applied on the amplification flexure P joint. In addition, assign same dimensions to the five notch hinges of the P joint, then the hinges' rotation angles around the z-axis are all the same values, namely, θ. Then, the potential energy of the P joint due to elastic deflections can be written as:

$$P_p = \frac{1}{2}K_2 u_x^2 = 5 \times \frac{1}{2}k\theta^2 \tag{2}$$

where

$$k = \frac{2Ewt^{2.5}}{9\pi r^{0.5}} \tag{3}$$

is the rotation stiffness (see Paros and Weisbord [1965]) of the right circle flexure hinge around the z-axis direction, and the relationship between the small rotation angle θ

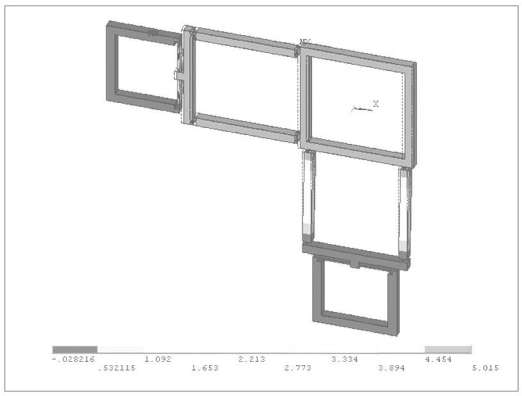

Fig. 12. The FEM of the original CPM.

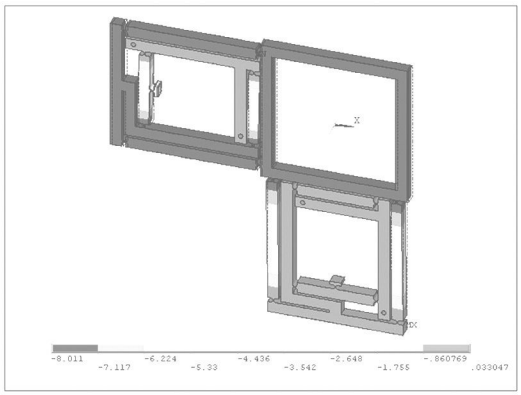

Fig. 13. The FEM of the improved CPM.

and the displacement u_x can be approximately expressed as:

$$u_x = l_2\theta. \tag{4}$$

Substituting (3) and (4) into (2) allows the calculation of the stiffness of the amplification P joint in y-axis direction:

$$K_2 = \frac{10Ewt^{2.5}}{9\pi r^{0.5} l_2^2}\ . \tag{5}$$

For an amplification of P joint with architectural parameters of $r = 2\,\text{mm}$, $t = 0.5\,\text{mm}$, $w = 10\,\text{mm}$, $l_1 = 72\,\text{mm}$, $l_2 = 36\,\text{mm}$, and $l_3 = 92\,\text{mm}$, the nonlinear statics analysis is performed with ANSYS, and the results are compared with the calculated ones as illustrated in Fig. 10. From the beeline plot of the FEA results, it can be conducted that the stiffening phenomenon has been eliminated from the modified CPM. However, the modified P joint introduces a parasitic motion along the y-axis as shown in Figs. 9 and 11. Even so, it will be shown later that this small motion does not increase parasitic motions of the final CPM.

Additionally, with reference to Fig. 8, the amplification ratio of the adopted P joint can be calculated as:

$$A_p = l_1/l_2 = 2. \tag{6}$$

In theory, the CPM workspace which takes on a cubic shape can be enlarged by a factor of $2^3 = 8$ times with the adoption of amplification mechanism. From the simulation results in Fig. 11, it is seen that the amplification ratio is 1.97, which is a little bit smaller than the theoretical one.

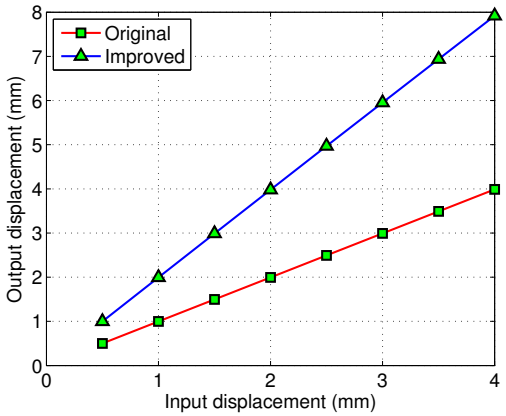

Fig. 14. Input and output displacement relationship of the two CPMs.

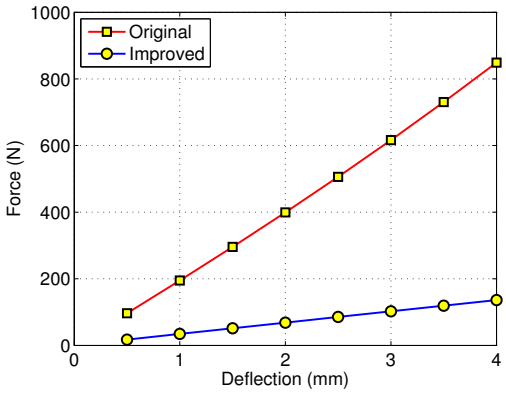

Fig. 15. Force-displacement relationship of the two CPMs.

This comes from the reason that the elements other than notch hinges are not fully rigid bodies.

4.2 Performance of the CPM

In order to demonstrate the merits of the improved CPM, both the original and current CPM with the same dimensions are analyzed via nonlinear statics FEA. In the simulation, the same displacements (5 mm) are assigned as inputs to the CPM, and the corresponding loads can be generated after the solution. Besides, the output motion of the mobile platform for the CPM can be generated as well.

The deformed finite element models (FEM) of the original and modified XY CPM are depicted in Figs. 12 and 13, respectively. And the relationships between the input and output displacements for the two CPMs are plotted in Fig. 14. It is found that with the same input displacements of linear actuators, the ratio of output displacements between the modified and original CPM is about 1.99, which is larger than 1.97 due to the stiffening phenomenon in the original CPM. Thus, the CPM workspace has been enlarged by almost 8 times. Moreover, it is observed that the modified CPM requires only about one sixth of forces from the actuator accordingly as illustrated in Fig. 15.

In addition, the parasitic motions versus the output displacements for the two CPMs are elaborated in Figs. 16 and 17, respectively. For the same value of output displacement $u_x = 4\,\text{mm}$, the parasitic motions along the

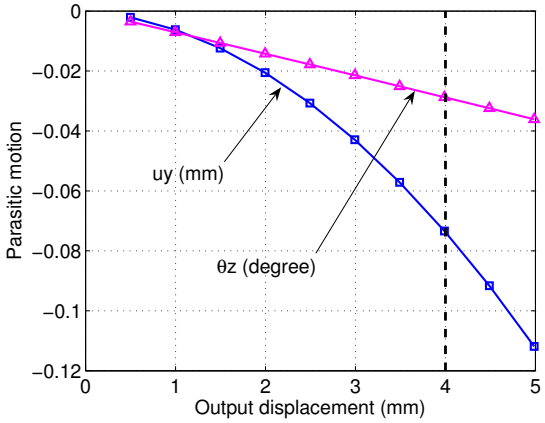

Fig. 16. Relationships between the output motion and parasitic motion of the original CPM.

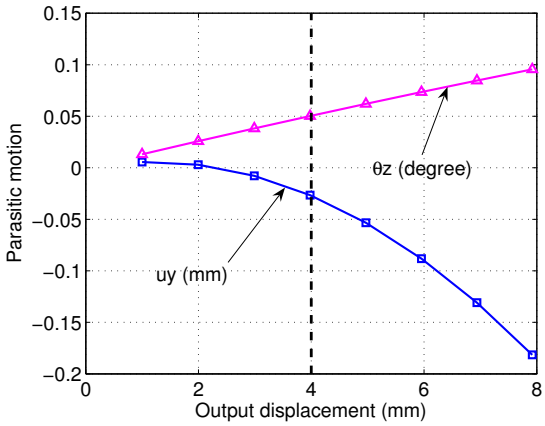

Fig. 17. Relationships between the output motion and parasitic motion of the improved CPM.

y-axis and around the z-axis, i.e., u_y and θ_z, are plotted in the figures. It can be observed that with respect to the same output displacement u_x, the crosstalk or parasitic translation of the platform in the y-axis direction of the improved CPM ($u_y = 26\,\mu$m) is smaller than that of the original CPM (($u_y = 75\,\mu$m)). An additional observation of the parasitic rotation reveals that the improved CPM has a slight larger rotation ($\theta_z = 0.050$ degree) around the z axis than the original CPM ($\theta_z = 0.029$ degree) around the inverse direction.

However, the parasitic rotation (0.05 degree) is very small, so that it can be neglected for the translational CPM. Moreover, the parasitic translation has been reduced by almost three times, and the maximum crosstalk for the improved CPM is only 0.65%. Hence, it can be taken as a decoupled XY stage approximately.

Indeed, the crosstalk of the designed CPM between the working axes will be fully compensated by a feedback controller for such practical applications as biological cell manipulation and so on.

5. CONCLUSION

The kinematic architecture of a high precision XY CPM featuring flexure hinges is improved in this paper. The evolution procedures of the CPM structure have been presented in details. And the advantages of the performance of the resulted CPM has been demonstrated by resorting to the FEA with ANSYS, which shows that the improved XY micromanipulator can provide nearly decoupled translations with motion range enlarged greatly while with the stress stiffening and buckling risks significantly diminished. The generated CPM is expected to find its way into micro and nano scale manipulation applications.

In our future work, a prototype of the designed CPM will be fabricated and its performances in terms of positioning resolution and repeatability will be tested as well.

REFERENCES

K.-S. Chen, D.L. Trumper, and S.T. Smith. Design and control for an electromagnetically driven X-Y-θ stage. *Precis. Eng.*, 26(4):355–369, 2002.

Y.-J. Choi, S.V. Sreenivasan, and B.J. Choi. Kinematic design of large displacement precision XY positioning stage by using cross strip flexure joints and over-constrained mechanism. *Mech. Mach. Theory*, 2007. In press.

Y. Li and Q. Xu. A novel design and analysis of a 2-DOF compliant parallel micromanipulator for nanomanipulation. *IEEE Trans. Automat. Sci. Eng.*, 3(3):248–254, 2006.

T.-F. Lu, D. C. Handley, Y. K Yong, and C. Eales. A three-DOF compliant micromotion stage with flexure hinges. *Ind. Robot*, 31(4):355–361, 2004.

J.-P. Merlet. *Parallel Robots*. Kluwer Academic Publishers, London, 2000.

K.-K. Oh, X.-J. Liu, D.S. Kang, and J. Kim. Optimal design of a micro parallel positioning platform. part II: Real machine design. *Robotica*, 23(1):109–122, 2005.

J.M. Paros and L. Weisbord. How to design flexure hinges. *Machine Design*, 37:151–156, 1965.

E. Pernette, S. Henein, I. Magnani, and R. Clavel. Design of parallel robots in microrobotics. *Robotica*, 15(4):417–420, 1997.

J.W. Ryu, D.-G. Gweon, and K.S. Moon. Optimal design of a flexure hinge based XYθ wafer stage. *Precis. Eng.*, 21(1):18–28, 1997.

T. Sievers and S. Fatikow. Real-time object tracking for the robot-based nanohandling in a scanning electron microscope. *J. Micromechatronics*, 3(3):267–284, 2006.

X. Tang and I.-M. Chen. A large-displacement 3-DOF flexure parallel mechanism with decoupled kinematics structure. In *Proc. IEEE/RSJ Int. Conf. on Intelligent Robots and Systems*, pages 1668–1673, 2006.

T. Tanikawa and T. Arai. Development of a micro-manipulation system having a two-fingered micro-hand. *IEEE Trans. Robot. Automat.*, 15(1):152–162, 1999.

Q. Xu and Y. Li. Design modification of a 3-PRC compliant parallel micromanipulator for micro/nano scale manipulation. In *Proc. 7th IEEE Conf. Nanotechnology*, pages 426–431, 2007.

Q. Yao, J. Dong, and P.M. Ferreira. Design, analysis, fabrication and testing of a parallel-kinematic micropositioning XY stage. *Int. J. Mach. Tools Manuf.*, 47(6): 946–961, 2007.

B.-J. Yi, G.B. Chung, H.Y. Na, W.K. Kim, and I.H. Suh. Design and experiment of a 3-DOF parallel micromechanism utilizing flexure hinges. *IEEE Trans. Robot. Automat.*, 19(4):604–612, 2003.